JOURNAL OF MATERIALS SCIENCE **40** (2005) 5669–5674

Acoustic emission study of corrosion fatigue crack propagation mechanism for LY12CZ and 7075-T6 aluminum alloys

H. CHANG
Environmental Corrosion Center, Institute of Metal Research, Chinese Academy of Sciences, Shenyang, 110016, China; Materials Science and Engineering College, Shenyang Ligong University, Shenyang, 110168, China

E. HAN, J. Q. WANG, W. KE
Environmental Corrosion Center, Institute of Metal Research, Chinese Academy of Sciences, Shenyang, 110016, China

Published online: 25 August 2005

Acoustic emission signals were continuously monitored during fatigue crack propagation for LY12CZ and 7075-T6 aluminum alloys in laboratory air and 3.5% NaCl solution. The results showed that the acoustic emission count rate was as a linear function of crack propagation rate during fatigue and corrosion fatigue. The acoustic emission activity for LY12CZ was smaller in solution than that in air; but for 7075-T6, greater in solution than that in air. The acoustic emission waveform parameter, the frequency centroid ratio, was tried to use as a criterion to distinguish the corrosion fatigue crack propagation mechanism for anodic dissolution of LY12CZ and hydrogen embrittlement of 7075-T6.

1. Introduction

Although acoustic emission (AE) technique has been used extensively to study fracture and fatigue and has been considered a promising technique already some thirty years ago, there are several factors preventing the advancement of this technique. One of theses factors is source pattern recognition, as there exist some difficulty in characterizing parameters. Furthermore, the sensors typically need are such that it is not possible to measure the complete waveform [1]. The development of the full waveform numeric AE systems and wideband sensors solve this problem [1–3].

Up to the present time there are many models for the mechanism of environmental sensitive cracking, including stress corrosion crack (SCC) and corrosion fatigue (CF) for precipitation hardened aluminum alloys. For aqueous solutions, crack growth is either controlled by anodic dissolution [4] or hydrogen embrittlement [4, 5–7] at the crack tip. It is now generally accepted that SCC of Al-Cu alloy in Cl^- containing aqueous solutions is controlled by an anodic dissolution mechanism [8–10]. During CF however, the crack tip strain rate changes with cyclic loading, which causes the mechanism of crack propagation to be more complex, but most of study for the corrosion fatigue crack propagation mechanisms of Al-Cu alloys in Cl^- solutions prefer to anodic dissolution mechanism [11, 12]. For the high strength 7075-T6 alloy, the CF mechanism in solution is usually attributed to the hydrogen embrittlement mechanism [6, 7, 12] which explains the cleavage fracture morphology and considers that the hydrogen atoms formed by the cathodic partial reaction to embrittle, the aluminum alloys by dislocation transmission and weakening the grain boundaries [6]. It is known that CF mechanisms for LY12CZ and 7075-T6 aluminum alloys are different, but there is no existing criterion to distinguish them.

In this paper, AE monitored CF tests were performed for LY12CZ and 7075-T6 aluminum alloys in order to find a criterion to distinguish, the two different crack propagation mechanisms by characteristic parameters and waveform analysis of AE signals.

2. Experimental procedure

The chemical composition and the mechanical properties of the alloy are listed in Table I. The single edge notched plate specimens (length = 250 mm, width = 36 mm and thickness = 2 mm) with a 5 mm precrack were cut by Mo line from rolled plate along the rolling direction. Testing was carried out in an INSTRON servo-mechanical fatigue testing machine with tension–tension sinusoidal loading at stress ratio R of 0.1 and frequency of 1 Hz in ambient laboratory air (temperature: 20–25°C). The crack length was measured at one side of the specimen using a traveling microscope with a magnification of 30 and 0.01 mm precision. Environmental test conditions were air and 3.5% NaCl aqueous solution.

0022-2461
DOI: 10.1007/s10853-005-1300-9

TABLE I. Composition (wt%) and mechanical properties of the two aluminum alloys

Material	Cu	Mg	Mn	Fe	Si	Zn	Ti	Cr	σ_YMPa	σ_{UTS}MPa	Elongation
LY12CZ	4.36	1.49	0.46	0.25	0.14	0.07	0.01		345	465	17.5%
7075-T6	1.2–2.0	2.1–2.9	0.3	0.5	0.4	5.1–6.1	0.2	0.18–0.28	469	538	7.0%

AE measurements were performed using AE equipment (DiSP system) manufactured by the Physical Acoustic Corporation. Two wideband transducers (WB) at a distance of 80 mm from the crack were symmetrically mounted on both sides of the pre-crack so that AE signal from the crack could be differentiated from the grip noise. AE signals from the two transducers were amplified by preamplifiers (40 dB), and then sent to the DiSP microprocessor. The WB transducers were broadband, high-fidelity and high sensitivity. These preamplifier outputs were bandpassed filtered from 20 KHz to 2 MHz. The threshold was 26 dB. The voltage time gate was utilized to control the stress phase of the loading cycle. During the tests, the AE signals were only accepted for the load range of above 0.7 maximum stress when there was crack closure. AE signal were measured with crack lengths from 5.0 to 20.0 mm. Subsequently the specimen was rapidly pulled to failure, and the morphologies of the fracture surfaces were examined using scanning electron microscopy (SEM).

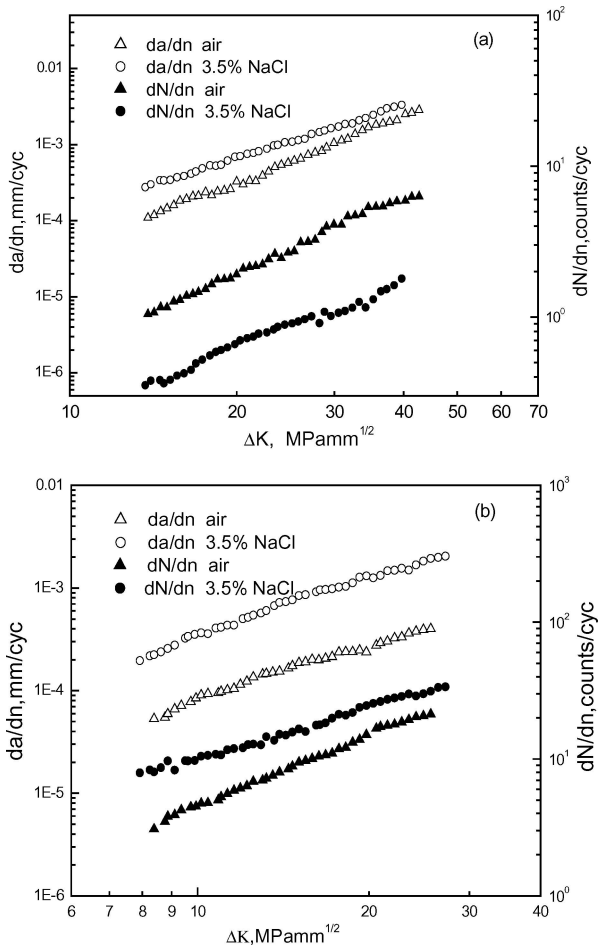

Figure 1 Relationships between the crack propagation rate (left-hand, with unfilled markers), the AE count rate (right-hand, with filled markers) and the stress intensity factor range for (a) LY12CZ and (b) 7075-T6 aluminum alloy in air and 3.5% NaCl solution.

3. Results

The fatigue crack propagation rate was chosen to be located in the second stage of the *da*/*dn* versus ΔK curve. It obeyed the Paris law [13], for crack growth (*da*) per cycle (*dn*):

$$da/dn = c \cdot (\Delta K)^m \tag{1}$$

where *c, m* are material constants. The AE count rare, amplitude and waveform of AE were analyzed during fatigue and CF. Fig. 1 shows the relationship between the crack propagation rate (*da*/*dn*), AE count rate (*dN*/*dn*), and the stress intensity factor range (ΔK) for (a) LY12CZ and (b) 7075-T6 aluminum alloys. The AE count rate (*dN*/*dn*) and the crack propagation rate (on log-log axes) increased almost linearly for the two aluminum alloys in both air and the solution. For LY12CZ aluminum alloy in corrosive solution the crack propagation rate (*da*/*dn*) increased and the AE count rate (*dN*/*dn*) decreased relative to in air. But for 7075-T6 aluminum alloy in solution, both *da*/*dn* and d*N*/*dn* increased relative to in air. The relationship between *da*/*dn* and d*N*/*dn* is shown in Fig. 2 for (a) LY12CZ and (b) 7075-T6 aluminum alloys. This relationship follows a linear law (on log-log axes) in the two environments. Furthermore, the AE count rate in air was larger than that in 3.5% NaCl solution at a given crack propagation rate. For LY12CZ the slopes of two lines were almost the same, but for 7075-T6 the difference of slopes was significant.

The amplitude distribution of the AE events for the two aluminum alloys in the two environments, shown in Fig. 3a, indicates that there were fewer AE signals in solution than air for LY12CZ, whereas for 7075-T6 there were more signals in solution than in air. Fig. 3b shows the logarithm slope of amplitude distribution. For the two alloys the slopes were similar in air and in solution.

Fig. 4 represents the average of 10 waveforms and Fast Fourier Transform Algorithm (FFT) spectra from fatigue crack growth for LY12CZ and 7075-T6 aluminum alloys in air. The average waveforms exhibited similar shape, and their FFT spectra were also similar. The peak frequency is at about 100 kHz, which reveals that the signals of fatigue crack propagation for LY12CZ and 7075-T6 aluminum alloys are from the same source. However, the corresponding average signals from corrosion fatigue crack propagation for the two aluminum alloys in 3.5% NaCl solution showed two distinctly different waveform shapes as shown in Fig. 5a and b. The FFT spectrum of average waveform for 7075-T6 aluminum alloy (Fig. 5d) has a wider frequency range than for LY12CZ aluminum alloy (Fig. 5c), and the peak frequencies were 100 kHz and 215 kHz respectively. The different peaks corresponded to different corrosion fatigue crack propagation mechanisms.

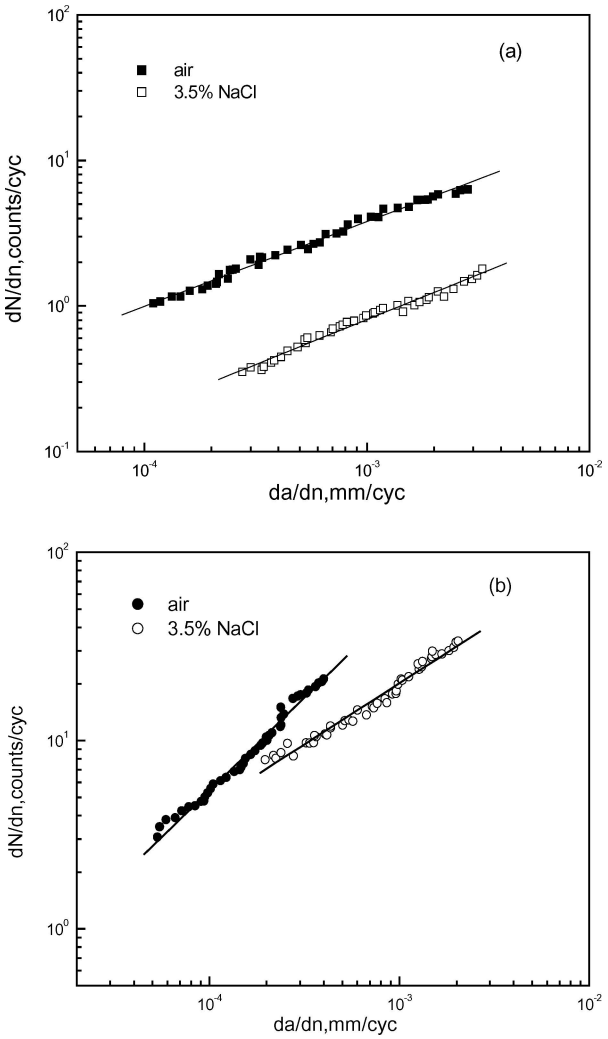

Figure 2 Relationship between AE count rate and crack propagation rate for (a) LY12CZ and (b) 7075-T6 aluminum alloys in air and 3.5% NaCl solution.

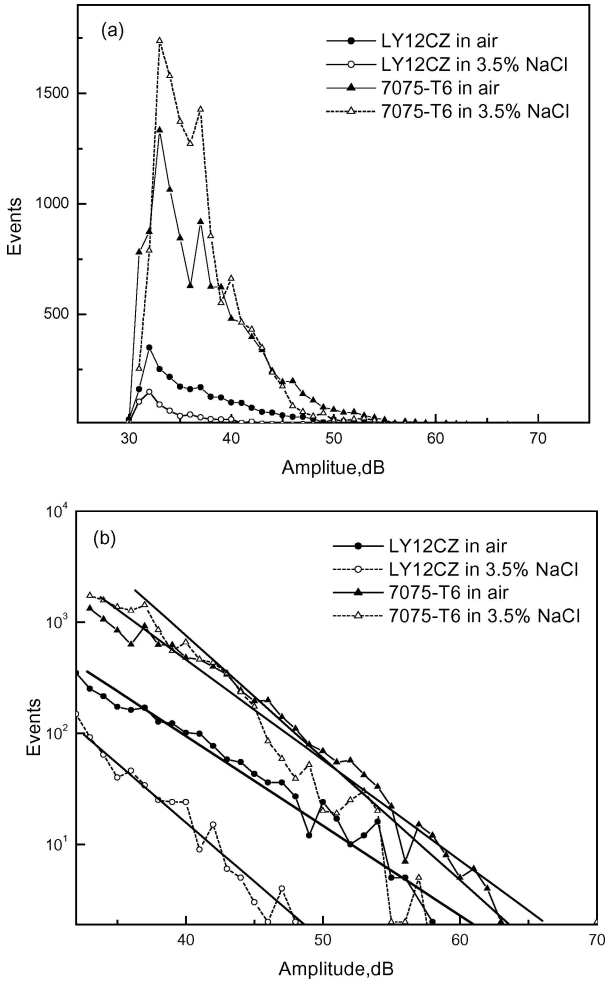

Figure 3 AE events vs amplitude (a) and its logarithm slope (b) for two aluminum alloys in air and 3.5% NaCl solution.

Fig. 6 shows scanning electron micrographs of the fatigue fracture surface for the LY12CZ aluminum alloy in (a) air and (b) 3.5% NaCl solution. The LY12CZ aluminum alloy had a ductile fracture surface both in air and in the 3.5% NaCl solution. The fracture surfaces for the 7075-T6 aluminum alloy are shown in Fig. 7. In air the fracture surface was similar to that for LY12CZ, but in the 3.5% NaCl solution the fracture surface was characterized by a cleavage brittle striation morphology.

4. Discussion

If the fatigue crack propagation was described by equation (1) Morton *et al*. [14, 15] found that the AE during fatigue crack propagation could be expressed by a similar equation:

$$dN/dn = c_1 \cdot (\Delta K)^{m_1} \tag{2}$$

where c_1 and m_1 are material constants. The relationship between crack propagation rate (da/dn) and AE counts rate (dN/dn) could be deducted from Equations 1 and 2:

$$dN/dn = \frac{c_1}{c^{m_1/m}}(da/dn)^{m_1/m}$$
$$dN/dn = c'(da/dn)^{m'} \tag{3}$$

where $c' = c_1/c^{m_1/m}$, $m' = m_1/m$. So the relationship between dN/dn and da/dn is linear in logarithm coordinates, which is consistent with the experiment results shown in Fig. 1.

It is known that the main AE source in fatigue is the energy release from the formation of the new surface by breaking atomic bonds and the change of the plastic zone at the crack tip during crack growth at the peak load [16]. Wang *et al*. [17] particularly discussed the relationship between the AE total counts and the change of the size of the plastic zone at the crack tip for low strength steel during CF, and proposed the model of the relation between $N\sigma_y$ and $N\gamma_p$, where $N\sigma_y$ is the increasing value of AE caused by the increase of material strength due to embrittlement at the crack tip and $N\gamma_p$ is the decreasing value of AE caused by the decrease of plastic zone size at the crack tip.

For LY12CZ, the AE count rate dN/dn was lower in solution than in air as shown in Fig. 1a; and the AE events were lower in solution than that in air as shown in Fig. 3a, which indicated that corrosion of the crack

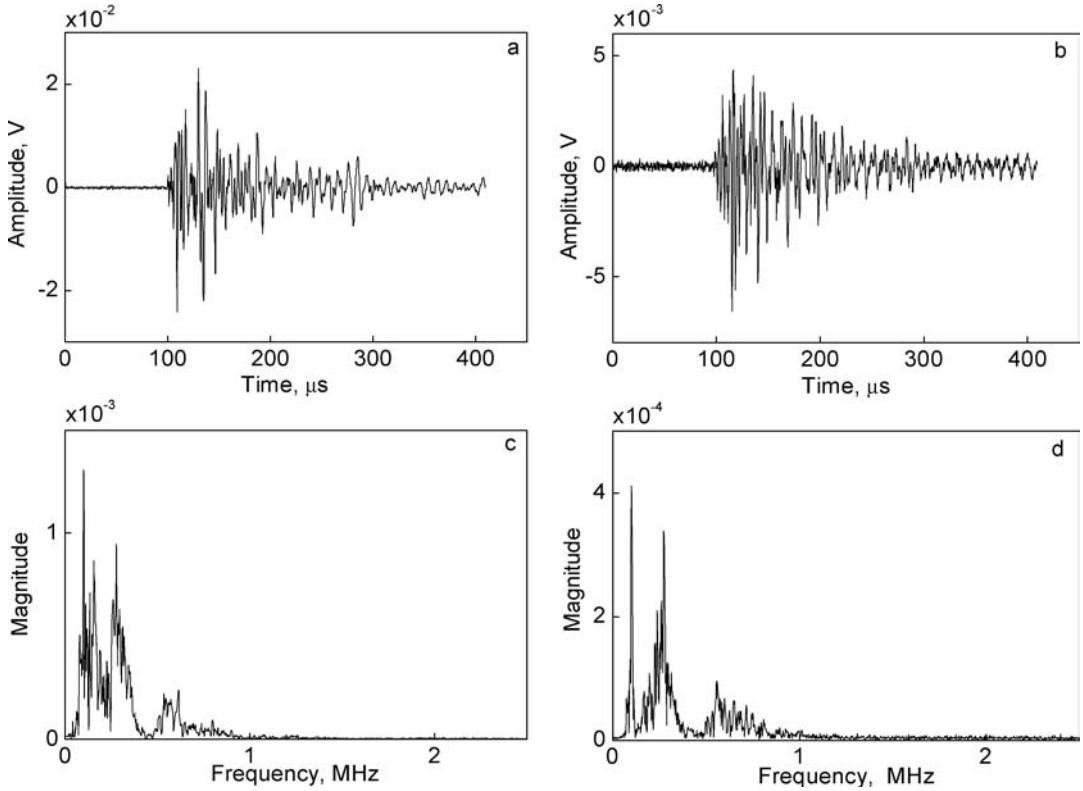

Figure 4 The average of 10 waveforms and FFT spectra from fatigue crack growth for LY12CZ (a, c) and 7075-T6 (b, d) in air.

tip did not only reduce AE counts but also weaken the AE activity. The slopes between *dN*/*dn* and *da*/*dn* were same in solution and air as shown in Fig. 2a, which is about 0.60. The average of waveforms and FFT spectra as shown in Figs. 4a, c and 5a, c also show that the sources of AE signals for LY12CZ were same both in air and solution. The fracture surface of LY12CZ as shown in Fig. 6 indicated the fracture modes were same in both air and solution. There were fatigue striations and micro-void on the facture surfaces. There was no evidence of breakdown of atomic bonds by cleavage for LY12CZ, so the reduction of the AE events

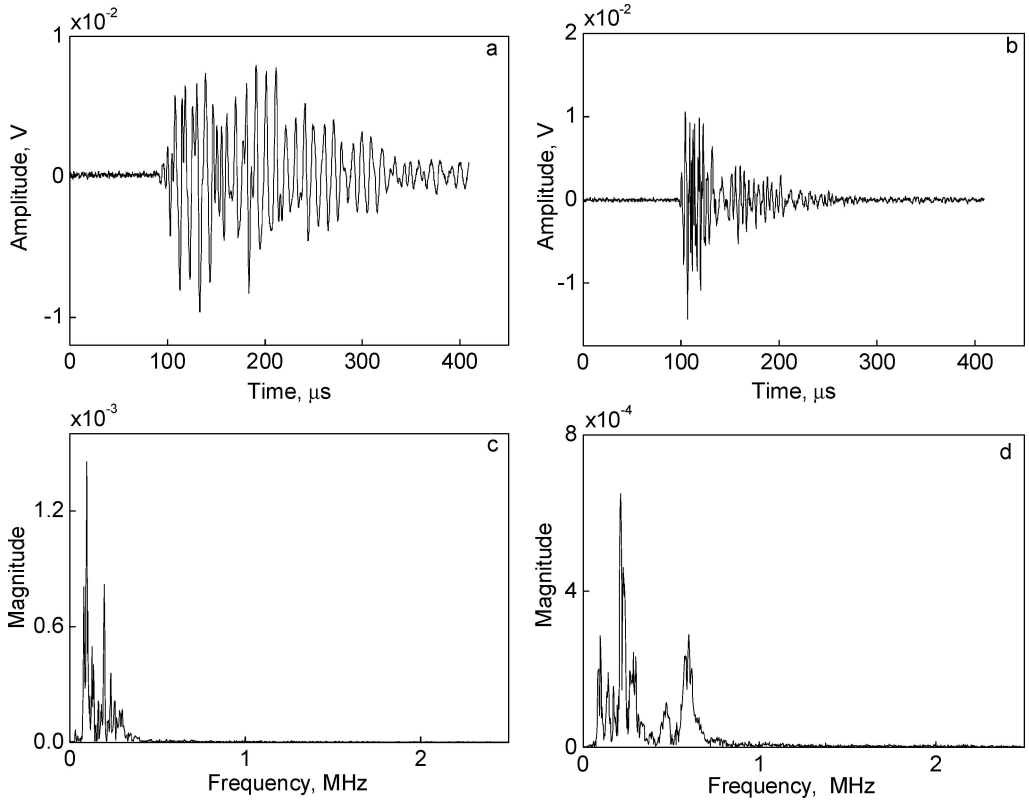

Figure 5 The average of 10 waveforms and FFT spectra from corrosion fatigue crack growth for LY12CZ (a, c) and 7075-T6 (b, d) in 3.5% NaCl solution.

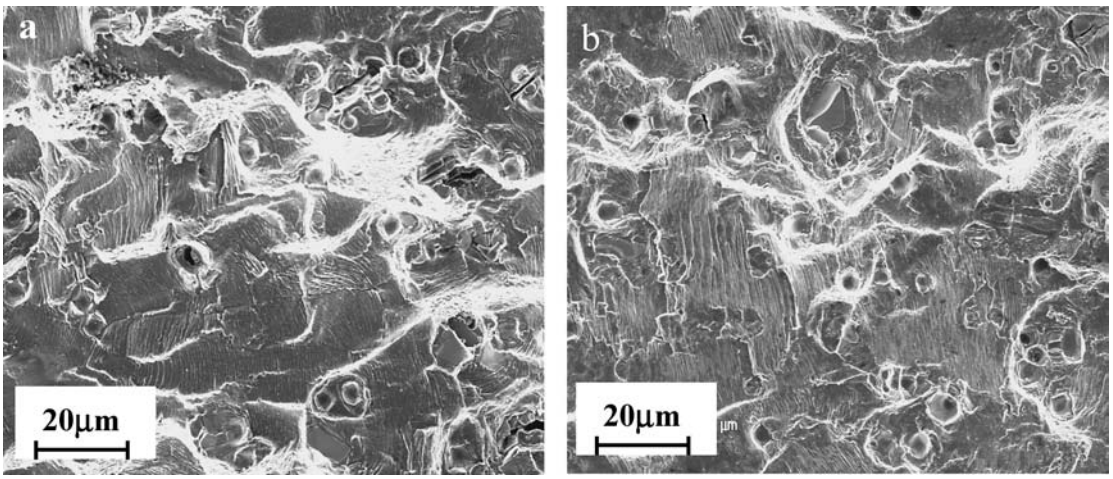

Figure 6 Scanning electron micrographs of fracture surfaces for the LY12CZ aluminum alloys (a) in air and (b) in 3.5% NaCl solution.

during CF crack propagation was mainly associated with the change of the size of the plastic zone at the crack tip. $N\sigma_y < N\gamma_p$, i.e., the decrease of the plastic zone played an important role during CF of LY12CZ. The mechanism of CF for LY12CZ was anodic dissolution affected the plastic zone size of crack tip.

Compared to LY12CZ, the high strength aluminum alloy 7075-T6 showed different AE behavior. AE count rate was higher in solution than that in air as shown in Fig. 1b; and AE activity was bigger in solution than that in air as shown in Fig. 3a. The slopes between *dN*/*dn* and *da*/*dn* in solution and air were different as shown in Fig. 2b. These were about 0.97 in air and 0.65 in the solution, respectively. The average of waveforms in air was very different to that in solution as shown in Figs 4b and 5b, and the peak frequency was 100 kHz in air (Fig. 4d) and 215 kHz in solution (Fig. 5d), which indicated that the source of AE signals in air was different to that in solution. Fig. 7b shows the fracture surface in solution was brittle with features of cleavage, cleavage steps and detachment at inclusions. These characteristics can be related to an abrupt energy release, to which AE is sensitive. This brittle fracture was attributed to the presence of hydrogen inside the crack and the entrance of hydrogen into the plastic zone in front of the crack tip. The alloy can be thus embrittled by hydrogen and this embrittlement provided an increasing $N\sigma_y$ and a large AE activity. The interaction of environments (dissolution or hydrogen embrittlement), mechanical conditions (triaxial stress) and material nature are considered to be the AE sources.

Frequency centroid (FC, in kHz) is one of waveform parameters of the AE signal and a real time frequency derived feature. The FC results from performing a real-time FFT and carrying out the following calculation on each FFT element:

$$FC = \text{SUM}(\text{magnitude} * \text{frequency}) / \text{SUM}(\text{magnitude}) \quad (4)$$

In order to embody the different frequency distribution character of the FFT spectra from CF crack propagation waveform for two aluminum alloys, the frequency range was divided into two parts: a high pass (*HP*) section: 400–1000 kHz; and a low pass (*LP*) section: 20-400 kHz. The frequency centroid ratio (*FCR*) is defined as:

$$FCR = FC_{HP}/FC_{LP} \quad (5)$$

FCR considered not only the magnitude but also the frequency distribution of signals. The different source of AE signal causes the different distribution of FCR. Fig. 8 shows the frequency centroid ratio (FCR)

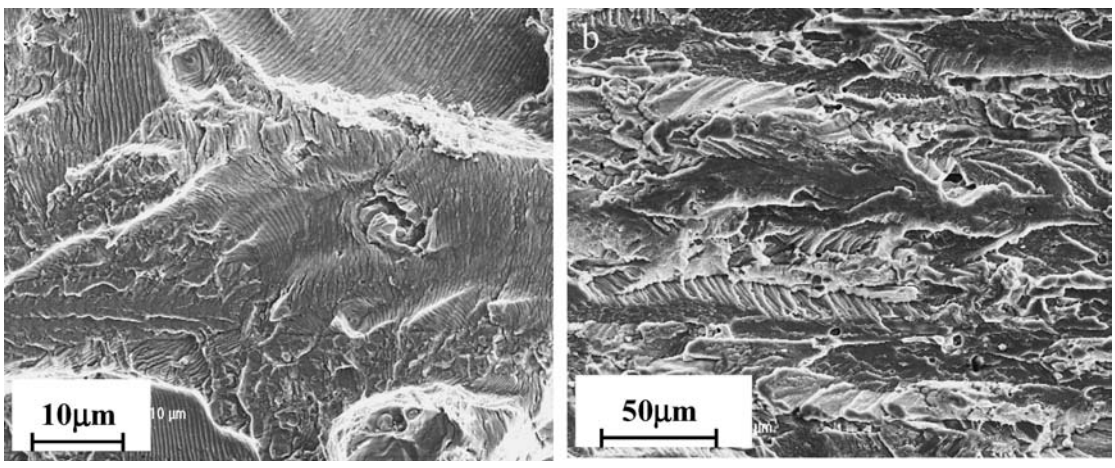

Figure 7 Scanning electron micrographs of fracture surfaces for the 7075-T6 aluminum alloys (a) in air and (b) in 3.5% NaCl solution.

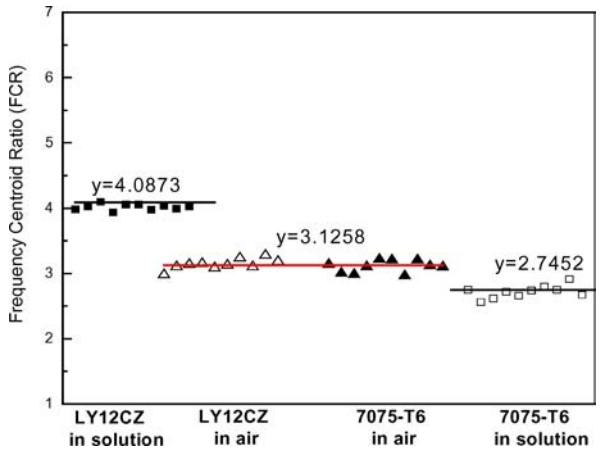

Figure 8 Frequency centroid ratio distribution of signals from fatigue and corrosion fatigue crack growth for LY12CZ and 7075-T6 in air and 3.5% NaCl solution.

distribution of 10 signals from crack propagation for LY12CZ and 7075-T6 aluminum alloys both in air and 3.5% NaCl solution. The FCR values were 3.1258 for LY12CZ and 7075-T6 in air, which is consistent with the result as shown in Fig. 4 that indicated the AE signal sources were same for LY12CZ and 7075-T6 loaded in air. The FCR values were about 4.0873 for LY12CZ, and 2.7452 for 7075-T6 in the 3.5%NaCl solution. The FCR distributions for LY12CZ in 3.5% NaCl solution was greater than that in air, however, for 7075-T6 it was smaller than that in air. It indicates when the sources of AE were plastic distortion (LY12CZ and 7075-T6 crack growth in air and LY12CZ in solution), the FCR distribution increased with the increasing embrittlement of crack tip, which was related to the essence of waveform and transmit of AE signals. When the crack propagation is controlled by hydrogen embrittlement mechanism, for 7075-T6 in solution, FCR distribution decreased with the increasing embrittlement of crack tip. So FCR is possible to be used as a criterion to distinguish corrosion fatigue crack propagation mechanisms, i.e., anodic dissolution for LY12CZ and hydrogen embrittlement for 7075-T6 aluminum alloys.

Of course, further experiments should be carried out in order to determine the possible FCR distribution of other materials whose corrosion fatigue crack propagation mechanisms are well-controlled by anodic dissolution or hydrogen embrittlement mechanisms, for instance: Al-Mg alloys crack growth in Cl^- and SO_4^{2-} solution (anodic dissolution mechanisms [18, 19]), other 7000 series alloys crack growth in NaCl solution (hydrogen embrittlement mechanisms [20]). Then it may be able to find a range or a boundary of FCR for crack propagation mechanisms controlled by anodic dissolution and hydrogen embrittlement mechanism. A thorough study of the acoustic emission for corrosion fatigue crack propagation mechanisms will be meaningful.

5. Conclusions

AE activity during fatigue crack propagation of two aluminum alloys was different in air and 3.5% NaCl solution. For LY12CZ, the activity was lower in 3.5% NaCl solution than that in air, and AE came mainly from plastic deformation at the crack tip during the fatigue process. But for 7075-T6, CF crack propagation controlled by hydrogen embrittlement dominated the AE source, so the activity was higher in the solution than in air.

Traditional amplitude distribution analysis can not distinguish the mechanism of CF crack propagation for the LY12CZ and 7075-T6 aluminum alloys. For the two alloys, the type of waveform and FFT spectra is similar during fatigue crack propagation but distinct during CF crack propagation. FCR was defined in this paper. The same source of AE signal induced the same FCR distribution. For anodic dissolution controlled CF, FCR value increased with the increasing embrittlement of crack tip; for hydrogen embrittlement controlled CF, it decreased with the increasing embrittlement of crack tip. It is possible to distinguish the CF crack propagation mechanism by analyzing the FCR distribution and the trend of its evolution in solution and air.

Acknowledgement

The work is funded by The Special Funds For The Major State Basic Research Projects **G19990650** of China and the Hundred Talent Project. The authors acknowledge the assistance

References

1. M. A. HAMSTAD and J. D. MCCOLSKEY, *J. Acoustic Emission.* **15** (1997) 1.
2. *Idem., Mater. Evalu.* **57** (1999) 1165.
3. K. ONO, *J. Acoustic Emission.* **15** (1997) S95.
4. F. P. FORD, *Corrosion.* **35** (1979) 281.
5. W. GRUHL, *Z. Metallkde.* **75** (1984) 819.
6. N. J. H. HOLROYD and D. HARDIE, *Corros. Sci.* **23** (1983) 527.
7. R. E. RICKER and D. J. DUQUETTE, *Metall. Trans: A*, **19A** (1988) 1775.
8. F. D. WALL and G. E. STONER, *Corros. Sci.* **39** (1997) 835.
9. K. URUSHINO and K. SUGIMOTO, *ibid.* **19** (1979) 225.
10. G. M. SCAMANS et al, *ibid.* **16** (1976) 443.
11. D. J. DUQUETTE, *AGARD Report*, No. AGARD-CP-316, 1981
12. F. P. FORD, *Corrosion.* **35** (1979) 281.
13. M. GAO, P. S. PAO and R. P. WEI, *Metall. Trans: A* **19A** (1988) 1739.
14. P. C. PARIS and F. ERDOGAN, *J. Basic Eng. Trans ASME (D).* **85** (1963) 528.
15. T. M. MORTON, S. SMITH and R. M. HARRINGTON, *Exp. Mech.* **14** (1974) 208.
16. T. M. MORTON, R. M. HARRINGTON and J. G. BJELETICH, *Eng. Fract. Mech.* **5** (1973) 691.
17. T. KISHI and Y. HISAMATSU, in Proc. 6th Acoustic Emission Symp. (Susono, Japan, JSNDI, 1982), p. 115.
18. Z. F. WANG, Z. ZHU and W. KE, *Metall. Trans: A.* **22A** (1991) 2677.
19. F. P. FORD, F. T. BURSTEIN and T. P. HOAR, *J. Electrochem. Soc.* **127** (1980) 1325.
20. N. J. H. HOLROYD and D. HARDIE, *Corros. Sci.* **23** (1983) 527.

Received 26 January
and accepted 17 March 2005